RSC Advances

PAPER

View Article Online
View Journal | View Issue

Cite this: *RSC Adv.*, 2015, **5**, 76675

Synthesized photo-cross-linking chalcones as novel corrosion inhibitors for mild steel in acidic medium: experimental, quantum chemical and Monte Carlo simulation studies

Baskar Ramaganthan,[ab] Mayakrishnan Gopiraman,[c] Lukman O. Olasunkanmi,[abd] Mwadham M. Kabanda,[ab] Sasikumar Yesudass,[ab] Indra Bahadur,[ab] Abolanle S. Adekunle,[abd] Ime B. Obot[e] and Eno E. Ebenso*[ab]

Received 23rd June 2015
Accepted 4th September 2015

DOI: 10.1039/c5ra12097g

www.rsc.org/advances

New chalcone derivatives namely (*E*)-(1-(5-(4-(3-(4-methylphenyl)-3-oxoprop-1-enyl)phenoxy)pentyl)-1*H*-1,2,3-triazol-4-yl)methyl acrylate (CH-5), (*E*)-(1-(5-(4-(3-(4-methylphenyl)-3-oxoprop-1-enyl)phenoxy) hexyl)-1*H*-1,2,3-triazol-4-yl)methyl acrylate (CH-6) and (*E*)-(1-(5-(4-(3-(4-methylphenyl)-3-oxoprop-1-enyl) phenoxy)decyl)-1*H*-1,2,3-triazol-4-yl) methyl acrylate (CH-10) were synthesized and characterized by Fourier transform infrared (FT-IR) and nuclear magnetic resonance (NMR) spectroscopic techniques. Ultraviolet-visible (UV-vis) spectra of the synthesized compounds confirmed that the chalcones undergo photo-cross-linking upon irradiation with UV-light. Potentiodynamic polarization measurements showed that both the intact and photo-cross-linked chalcones are mixed-type corrosion inhibitors for mild steel in aqueous hydrochloric acid. The EIS results showed an increase in charge transfer resistance with increasing concentration of the inhibitors. The chalcone derivatives adsorb spontaneously on the mild steel surface and their adsorption obeyed the Langmuir adsorption isotherm. The adsorption mode revealed the possibility of competitive physisorption and chemisorption mechanisms. Scanning electron microscopy coupled with energy dispersive X-ray spectroscopy (SEM-EDX) analyses confirmed that the chalcones formed a protective film on the mild steel surface. The overall results showed that the photo-cross-linked chalcones are better corrosion inhibitors than the intact chalcones. The results of quantum chemical calculations and Monte Carlo simulation studies are in good agreement with experimental results.

1. Introduction

Mild steel (MS) is a popular alloy of iron with various applications in oil refineries, chemical and transportation industries among others. This is due to its excellent mechanical strength and relatively low cost compared to other metal alloys.[1,2] Many industrial activities such as acid pickling, chemical etching, cleaning of oil refinery equipment, oil well acidizing and acid descaling involve the use of aqueous solutions of mineral acids which constitute strong corrosive media for mild steel.[3–5] In order to control metal dissolution associated with these industrial activities, various types of inhibitors are usually employed. It is well known that organic compounds containing heteroatoms such as sulphur, nitrogen, oxygen and aromatic rings display good inhibition properties for metal corrosion in aggressive media.[6–9] However, many of the existing organic/inorganic corrosion inhibitors especially those that contain heavy metals and phosphates are highly toxic and not eco-friendly. As the quest for environmental friendly and/or non-toxic anticorrosion agents increases, studies on the development of new prospective efficient corrosion inhibitors that are free of heavy metals and organic phosphates are becoming sizeable.[10–12]

Chalcones are open-chain flavonoid compounds that exhibit interesting pharmacological activities.[13,14] The inhibitive actions of some chalcone derivatives on the corrosion of MS in acidic environments have been reported by Li *et al.*[15,16] However, information on the corrosion inhibition properties and the inhibition mechanism of many chalcone derivatives is still fragmentary. Chalcone derivatives are also known to exhibit excellent photo-cross-linking properties due to the presence of

[a]*Department of Chemistry, North-West University (Mafikeng Campus), Private Bag X2046, Mmabatho 2735, South Africa. E-mail: Eno.Ebenso@nwu.ac.za; Fax: +27 183892052; Tel: +27 183892050, +27 183892051*

[b]*Material Science Innovation & Modelling (MaSIM) Research Focus Area, Faculty of Agriculture, Science and Technology, North-West University (Mafikeng Campus), Private Bag X2046, Mmabatho 2735, South Africa*

[c]*Nano Fusion Technology Research Lab, Interdisciplinary Graduate School of Science and Technology, Shinshu University, Ueda, Nagano 3868567, Japan*

[d]*Department of Chemistry, Obafemi Awolowo University, Ile-Ife 220005, Nigeria*

[e]*Centre of Research Excellence in Corrosion, Research Institute, King Fahd University of Petroleum and Minerals, Dhahran 31261, Saudi Arabia*

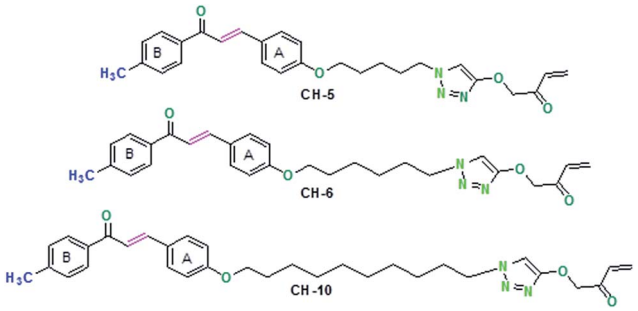

Fig. 1 The molecular structures of the studied chalcones: CH-5, CH-6, and CH-10.

α,β-unsaturated group, which undergoes [2π + 2π] cycloaddition reaction upon irradiating with UV light. Recently, our research group has developed a new perspective on corrosion inhibition of mild steel in acidic medium using triazole containing photo-cross-linking polymers.[17–19] 1,2,3-Triazoles are important class of five-membered nitrogen containing heterocycles with applications in various areas including organic synthesis, pharmaceutics, agrochemicals and dye industries. Their applications as corrosion inhibitors, photo-stabilizers and photo-graphic materials have also been reported.[20]

The present work focuses on the introduction of triazole moiety into chalcone derivatives. Triazole moiety possesses excellent corrosion inhibition efficiency, while chalcone derivatives exhibit good solubility, excellent processability, high thermal stability and environmental friendliness.[21–23] The work aims at combining the aforementioned interesting properties of these two families of compounds to produce some novel environmental friendly chalcone–triazole derivatives as potential corrosion inhibitors for MS in 1.0 M HCl solution. Electrochemical measurements, surface analyses, quantum chemical calculations and Monte Carlo simulations studies were carried out to investigate the adsorption and corrosion inhibition characteristics of the studied compounds. It is noteworthy to state that reports on adsorption and corrosion inhibition properties of chalcones using a combination of electrochemical techniques, quantum chemical calculations and Monte Carlo simulations are not common in literature. More so, the set of chalcone–triazole compounds used in this work are being reported as corrosion inhibitors for mild steel in 1 M HCl for the first time. The molecular structures of studied chalcones are given in Fig. 1.

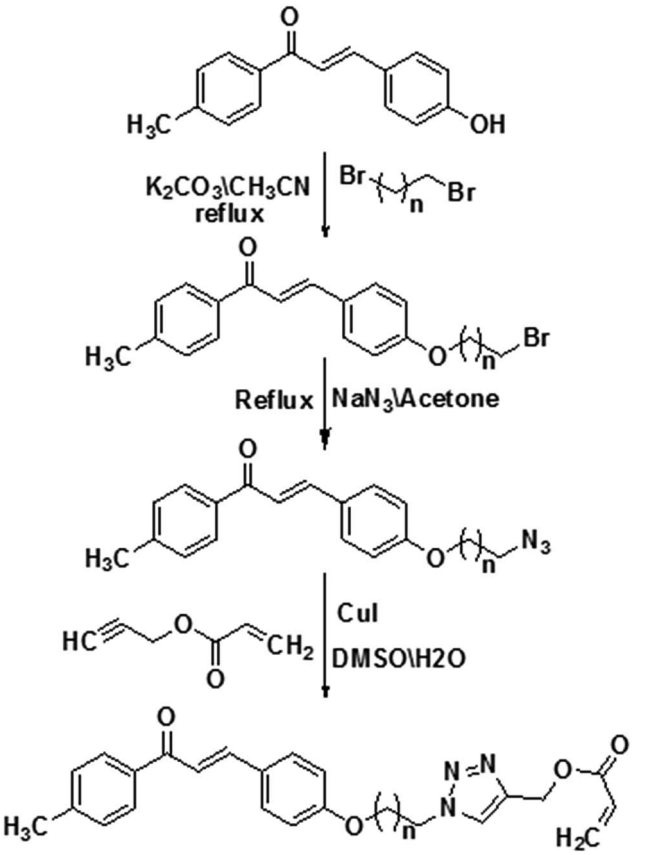

Fig. 2 Schematic diagram for the synthetic route of the chalcones: (n = 4 (CH-5), n = 5 (CH-6) and n = 9 (CH-10)).

2. Experimental procedures and computational details

2.1. Synthesis of the chalcone derivatives

The synthesis of the chalcone derivatives was carried out as previously reported.[17,24] A mixture of 4-hydroxybenzaldehyde (0.015 mol) and 4-methylacetophenone (0.015 mol) was put in 30 mL methanol after which potassium hydroxide (40%, 20 mL) was added slowly with constant stirring. After 6 h the reaction mixture was poured in ice cold water (500 mL) to obtain a yellow precipitate. The precipitate was filtered, washed several times in distilled water and dried. The precipitate was reacted with corresponding dibromoalkane in the presence of potassium carbonate (using acetonitrile as solvent) to produce (*E*)-3-(4-(3-bromoalkoxy)phenyl)-1-*p*-tolylprop-2-en-1-one, which was further reacted with sodium azide in acetone to obtain (*E*)-3-(4-(3-azidoalkoxy)phenyl)-1-*p*-tolylprop-2-en-1-one. The photo-cross-linking inhibitors were synthesized from (*E*)-3-(4-(3-azidoalkoxy)phenyl)-1-*p*-tolylprop-2-en-1-one and propargyl acrylate by click chemistry.[17]

All chemicals and reagents used for the synthesis were purchased from Merck and used without further purification. The schematic diagram of the overall synthetic route is presented in Fig. 2.

2.2. Characterization techniques

The synthesized chalcone derivatives were characterized using Fourier transform infrared (FTIR) and nuclear magnetic resonance (NMR) spectroscopic techniques. NMR spectra were recorded on BRUKER 500 MHz AVANCE III instrument using dimethyl sulfoxide-D6 as solvent and tetramethylsilane as internal standard. Fourier transform infrared (FT-IR) spectra were obtained on Perkin Elmer Spectrum 1 model, using KBr pellet method in the range 4000–400 cm^{-1} wavenumber.

2.2.1. Analytical data of the synthesized chalcone derivatives

CH-5 ((E)-(1-(5-(4-(3-(4-methylphenyl)-3-oxoprop-1-enyl)phenoxy)pentyl)-1H-1,2,3-triazol-4-yl)methyl acrylate). yield 76%; ^{1}H NMR (500 MHz, $CDCl_3$) δ ppm 1.52–158 (m, 2H), 1.70–1.76 (m, 2H), 1.84–1.94 (m, 2H), 2.45 (s, 3H) 4.06 (t, $J = 6.5$ Hz, 2H), 4.41 (t, $J = 7.0$ Hz, 2H), 5.33 (s, 2H), 5.88 (dd, $J = 10.5$ Hz, 1H), 6.15 (dd, $J = 16.5$ Hz, 1H), 6.47 (dd, $J = 16.0$ Hz, 1H) 6.94 (d, $J = 8.5$ Hz, 2H), 7.31 (d, $J = 8.0$ Hz, 2H), 7.44 (d, $J = 16.0$ Hz, 1H), 7.61 (d, $J = 8.5$ Hz, 2H), 7.80 (d, $J = 15.5$ Hz, 1H), 7.95 (d, $J = 7.5$ Hz, 2H), ^{13}C NMR (126 MHz, $CDCl_3$) δ ppm 21.60, 28.56, 28.91, 29.95, 52.32, 67.89, 114.85, 119.75, 127.37, 128.00, 128.57, 129.27, 130.18, 132.18, 135.92, 143.37, 144.29, 161.07, 190.09. IR (KBr, cm^{-1}) 738, 800, 811, 984, 1014, 1033, 1173, 1213, 1223, 1252, 1291, 1408, 1469, 1508, 1573, 1598, 1659, 1725, 2856, 2925, 3033, 3058, 3434.

CH-6 ((E)-(1-(5-(4-(3-(4-methylphenyl)-3-oxoprop-1-enyl)phenoxy)hexyl)-1H-1,2,3-triazol-4-yl)methyl acrylate). yield 77%; ^{1}H NMR (500 MHz, $CDCl_3$) δ ppm 1.42 (m, $J = 7.5$ Hz, 2H), 1.54 (m, $J = 7.0$ Hz, 2H), 1.81 (m, $J = 7.0$ Hz, 2H), 1.97 (m, $J = 8.0$ Hz, 2H), 2.45 (s, 3H) 4.00 (t, $J = 6.5$ Hz, 2H), 4.38 (t, $J = 7.0$ Hz, 2H), 5.32 (s, 2H), 5.86 (dd, $J = 10.5$ Hz, 1H), 6.15 (dd, $J = 16.5$ Hz, 1H), 6.45 (dd, $J = 17.0$ Hz, 1H), 6.92 (d, $J = 9.0$ Hz, 2H), 7.31 (d, $J = 8.0$ Hz, 2H), 7.44 (d, $J = 15.5$ Hz, 1H), 7.61 (d, $J = 9.0$ Hz, 2H), 7.78 (d, $J = 15.5$ Hz, 1H), 7.94 (d, $J = 8.0$ Hz, 2H), ^{13}C NMR (126 MHz, $CDCl_3$) δ ppm 21.66, 25.50, 26.22, 28.90, 30.16, 50.29, 57.75, 67.75, 114.79, 119.75, 123.52, 127.66, 128.01, 128.29, 129.27, 130.18, 131.49, 135.92, 142.86, 143.37, 144.26, 161.03, 190.07. IR (KBr, cm^{-1}) 736, 801, 810, 916, 978, 1015, 1030, 1175, 1222, 1252, 1292, 1409, 1460, 1508, 1573, 1606, 1658, 1722, 2863, 2938, 3035, 3085, 3129, 3432.

(CH-10) ((E)-(1-(5-(4-(3-(4-methylphenyl)-3-oxoprop-1-enyl)phenoxy)decyl)-1H-1,2,3-triazol-4-yl)methyl acrylate). Yield 74%; ^{1}H NMR (500 MHz, $CDCl_3$) δ ppm 1.32–1.39 (m, 10H), 1.45 (m, 2H), 1.78 (m, $J = 7.5$ Hz, 2H), 1.90 (m, 2H), 2.43 (s, 3H), 3.99 (t, $J = 6.5$ Hz, 2H), 4.33 (t, $J = 7.5$ Hz, 2H), 5.31 (s, 3H), 5.85 (dd, $J = 10.5$ Hz, 1H), 6.13 (dd, $J = 10.5$ Hz, 1H), 6.43 (dd, $J = 17.5$ Hz, 1H), 6.92 (d, $J = 9.0$ Hz, 2H), 7.29 (d, $J = 8.0$ Hz, 2H), 7.42 (d, $J = 15.5$ Hz, 1H), 7.58 (d, $J = 8.5$ Hz, 2H), 7.62 (s, 1H), 7.77 (d, $J = 15.5$ Hz, 1H), 7.92 (d, $J = 8.5$ Hz, 2H), ^{13}C NMR (126 MHz, $CDCl_3$) δ ppm 21.64, 25.95, 26.43, 28.92, 29.12, 29.25, 29.36, 30.21, 50.44, 57.74, 68.14, 114.90, 119.64, 123.71, 127.50, 128.01, 128.55, 129.26, 130.17, 131.47, 135.92, 142.82, 143.35, 144.36, 161.21, 166.03, 190.12. IR (KBr, cm^{-1}) 724, 736, 797, 807, 833, 983, 1014, 1042, 1174, 1223, 1263, 1292, 1408, 1469, 1513, 1570, 1606, 1663, 1722, 2850, 2919, 3032, 3082, 3123, 3433.

2.3. Materials and aggressive solutions for corrosion inhibition tests

MS specimens with the percentage by weight compositions of Mn (0.340%), C (0.100%), Cr (0.220%) and Fe (99.34%) were used for the corrosion inhibition studies. The MS coupons were abraded using emery papers of various grit sizes (400 to 1200) after which the specimens were washed thoroughly with double distilled water, degreased with acetone and dried at room temperature. The blank acid solution (1 M HCl) was prepared by dilution of analytical grade 37% HCl with double distilled water, while the aggressive solutions containing 5 to 15 ppm of the chalcone derivatives (inhibitors) were prepared by first dissolving appropriate amount of the compounds in 3.0 mL dimethylsulfoxide (DMSO) and then make up to 100 mL solution with 1.0 M HCl.

Photo-cross-linked chalcone derivatives were obtained by keeping 3.0 mL DMSO solution of the chalcone derivatives under high pressure (75 W) mercury lamp for 1 h. The compounds were confirmed to have photo-cross-linked after 1 h by using UV-vis spectrophotometer as explained later in Section 2.4. Various concentrations (5–15 ppm) of the photo-cross-linked chalcones used as corrosion inhibitors were also prepared in 1.0 M HCl.

2.4. Photochemical properties

Absorbance spectra of the synthesized chalcones were recorded on UV-1601 Shimadzu UV-vis spectrometer in the wavelength range of 200–800 nm using chloroform as solvent. The chalcones were tested for their photo-cross-linking ability by fixing the chloroform solutions of the compounds at a distance of 10 cm from a high pressure (75 W) mercury lamp and irradiate at regular time intervals with UV-vis spectrum being recorded immediately after each exposure. The chalcones were found to have photo-cross-linked after 1000 s.

2.5. Electrochemical techniques

Electrochemical measurements were carried out using CH electrochemical analyzer model 604B with conventional three electrode system. A square cut of MS coupon with surface area of 1 cm^2 was used as the working electrode. Platinum rod and saturated calomel electrode (SCE) were used as the counter and reference electrodes respectively. The surface of the MS used as working electrode was mechanically polished as earlier described in Section 2.3 above.

All the measurements were carried out in an aerated environment with continuous stirring at 300 $\pm$ 2 K. Potentiodynamic polarization measurements were carried out between -200 mV to -800 mV (*vs.* SCE) at the potential sweep rate of 0.5 mV s^{-1}. Electrochemical kinetic parameters such as corrosion current density (I_{corr}), anodic and cathodic Tafel slopes (b_a and b_c respectively) were obtained by extrapolating the linear Tafel regions of the polarization curves to corrosion potential (E_{corr}). Inhibition efficiency (IE%) was calculated using the equation:

$$\mathrm{IE}(\%) = \frac{I'_{corr} - I_{corr}}{I'_{corr}} \times 100 \quad (1)$$

where I'_{corr} and I_{corr} are corrosion current densities in the absence and presence of inhibitors respectively.[25] Electrochemical impedance spectroscopy (EIS) measurements were carried out in the frequency range from 100 kHz to 10 mHz at an amplitude of 10 mV.[26] The impedance spectra were fitted into the $R_s(R_{ct}CPE)$ equivalent circuit to obtain the EIS parameters and the inhibition efficiency (IE%) was calculated using the equation:

$$\mathrm{IE}(\%) = \frac{R_{ct} - R'_{ct}}{R_{ct}} \times 100 \quad (2)$$

where R'_{ct} and R_{ct} are charge transfer resistances in the absence and presence of inhibitors respectively.[27]

2.6. Surface analysis

In order to investigate the formation of protective film of the inhibitors on the steel surface, MS specimens were immersed in 1.0 M HCl solution without and with 15 ppm chalcone derivatives under the same conditions. The MS specimens used for the surface analysis studies were freshly abraded as previously discussed in Section 2.3 above. The MS specimens were removed after 2 h, washed with distilled water and air-dried. Scanning electron microscopy (SEM) and energy dispersive X-ray (EDX) spectrometry analyses of the MS surfaces were carried out using the FEI Quanta 200 F.

2.7. Computational details

2.7.1. Quantum chemical calculations. Quantum chemical calculations were performed to compute some parameters that describe the trend of reactivity of the inhibitor molecules towards adsorption on iron surface. Geometry optimizations were carried out on the intact chalcones (CH-5, CH-6 and CH-10) as well as their photo-cross-linked analogues (CH-5c, CH-6c and CH-10c). The dimerized structures of the respective chalcone derivatives resulting from their $2\pi + 2\pi$ addition reaction after UV-irradiation were used as the starting geometries for the photo-cross-linked chalcones. All geometry optimizations and quantum chemical calculations were performed using density functional theory (DFT) and the 6-31+G (d, p) basis set. The Becke's three parameter hybrid functional together with the Lee–Yang–Parr correlation functional (B3LYP),[28] was selected for the calculations. Some of the chemical parameters calculated include energy of the highest occupied molecular orbital (E_{HOMO}), energy of the lowest unoccupied molecular orbital (E_{LUMO}), global chemical hardness and softness. The global chemical hardness (η) is a measure of the resistance of an atom to a charge transfer.[29] It is calculated by using the equation:

$$\eta \cong -1/2(E_{HOMO} - E_{LUMO}) \quad (3)$$

The chemical softness (σ) describes the capacity of an atom or group of atoms to receive electrons[29] and is calculated as:

$$\sigma = 1/\eta \cong -2/(E_{HOMO} - E_{LUMO}) \quad (4)$$

All calculations were carried out using the Gaussian09 for Windows (G09W).[30] Schematic structures were drawn using the ChemOffice package in the UltraChem 2010 version while optimized structures were visualized with the GaussView 5.0 program.

2.7.2. Monte Carlo simulations. The Monte Carlo (MC) search was adopted to compute the low configuration adsorption energy of the interactions of the intact chalcone derivatives, CH-5, CH-6 and CH-10, and clean iron surface. Simulations of the photo-cross-linked chalcones could not be achieved due to their large sizes. Therefore, only the simulation results for the interactions between the intact chalcone derivatives and iron surface are presented and discussed in this study. For the whole simulation procedure, the Condensed-phase Optimized Molecular Potentials for Atomistic Simulation Studies (COMPASS) force field was used to optimize the structures of all components of the system of interest. The simulation was carried out with Fe (110) crystal with a slab of 5 Å in depth with periodic boundary conditions in order to simulate a representative part of an interface devoid of any arbitrary boundary effects. The Fe (110) plane was next enlarged to a (12 × 12) supercell to provide a large surface for the interaction of the inhibitors. After that, a vacuum slab with 50 Å thickness was built above the Fe (110) plane. The cleavage of Fe crystal along the (110) plane provides adequate representation of the Fe surface with sufficient stability and moderate atom density.[31–33] The Fe (110) plane has been successfully applied in literatures to describe the interactions between inhibitor molecules and Fe surface.[31,32,34] All simulations were carried out using Materials Studio 7.0 commercial software licensed from Accelrys Inc. USA.

3. Results and discussion

3.1. Characterization of the synthesized chalcone derivatives

FT-IR spectra of the synthesized chalcone derivatives (CH-5, CH-6 and CH-10) are shown in Fig. 3. The peaks at 2938 cm^{-1} and 2896 cm^{-1} can be assigned to the stretching vibrations of aromatic and aliphatic C–H groups respectively. Stretching bands of the ester C=O and α,β-unsaturated C=O were observed at 1722 cm^{-1} and 1606 cm^{-1} respectively. The peak at 1508 cm^{-1} is attributed to the stretching mode of aromatic C=C group and the band at 1175 cm^{-1} is attributed to the stretching of the triazole ring formed by click-chemistry. The C–C stretching and bending modes were observed at 1456 and 1072 cm^{-1} respectively while the band at 810 cm^{-1} is for the bending vibration of C–H.[35]

The ^{1}H NMR spectrum of the synthesized chalcone derivative (CH-10) is shown in Fig. 4. Since the synthesized chalcone

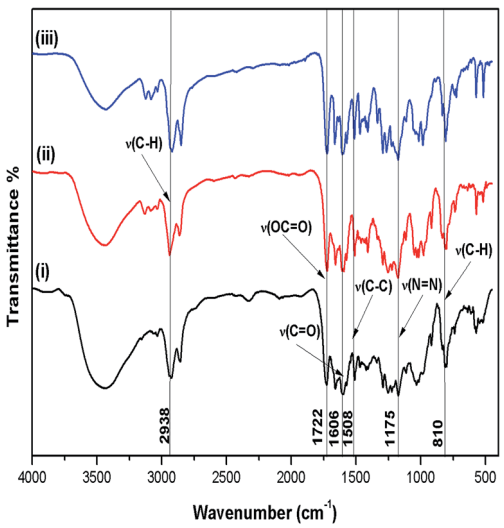

Fig. 3 FT-IR spectra of the synthesized chalcones: CH-5 (i), CH-6 (ii) and CH-10 (iii).

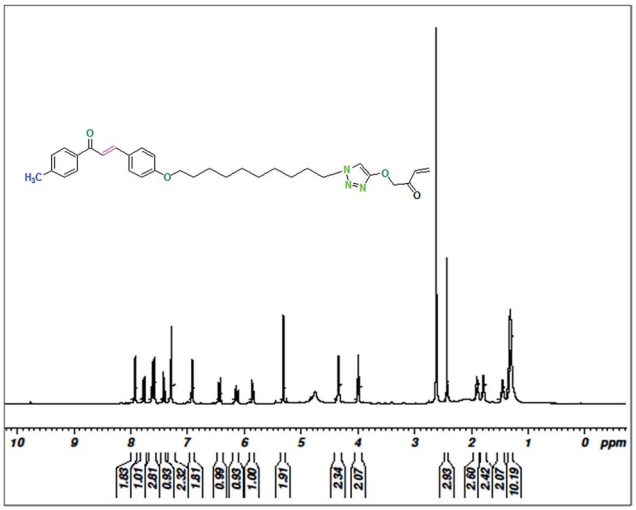

Fig. 4 ^{1}H NMR spectrum of CH-10.

derivatives only differ in the aliphatic chain, the ^{1}H NMR spectra of the other chalcone derivatives (CH-5 and CH-6 not shown) are similar to the one in Fig. 4 and the spectra data for the three chalcone derivatives have been listed in Section 2.2.1. The ^{1}H NMR spectra for all the synthesized chalcones show multiplets between 1.0 ppm and 2.5 ppm corresponding to the splitting of the aliphatic protons. The doublet at 3.90 ppm is assigned to the protons of the –O–CH_2– group that forms part of the aliphatic chain bridging the chalcone and triazole units, while the one at 4.2 ppm is assigned to the –CH_2– group directly attached to the nitrogen atom of the triazole ring. All the synthesized chalcone derivatives exhibit three doublets of doublets which correspond to the acrylate unit. The chalcone derivatives also showed two doublets at 7.42 (d, $J = 15.5$ Hz, 1H) and 7.78 (d, $J = 15.5$ Hz, 1H) ppm which are known to be characteristic peaks of chalcone moiety with the coupling constant (J) values that confirm the synthesized chalcones as *trans* isomers.[24]

3.2. Photo-cross-linking properties of the chalcone derivatives

The UV-vis absorption spectra of the chalcone derivatives before and after UV-irradiation are presented in Fig. 5. As shown in Fig. 5, the wavelength of maximum absorbance (λ_{max}) of all the three chalcone derivatives is 320 nm irrespective of the co-substituent, which suggests that the aliphatic chain linking the chalcone moiety to the triazole unit does not affect the absorption spectrum.[36] The UV-vis absorption characteristics of the synthesized chalcone derivatives are due to the $\pi \rightarrow \pi^*$ transition of the >C=C< group. The intensity of the absorption peak at 320 nm decreased rapidly upon UV-irradiation while the intensity of the one at 279 nm increased gradually. This observation is attributed to the formation of cyclobutane ring through $(2\pi + 2\pi)$ cycloaddition of the carbon–carbon double bond in the chalcone unit. An isosbestic point is observed at 270 nm due to *cis–trans* isomerization of the double bonds in the chalcones.[37] The absorption peak at 328 nm almost disappeared after irradiation

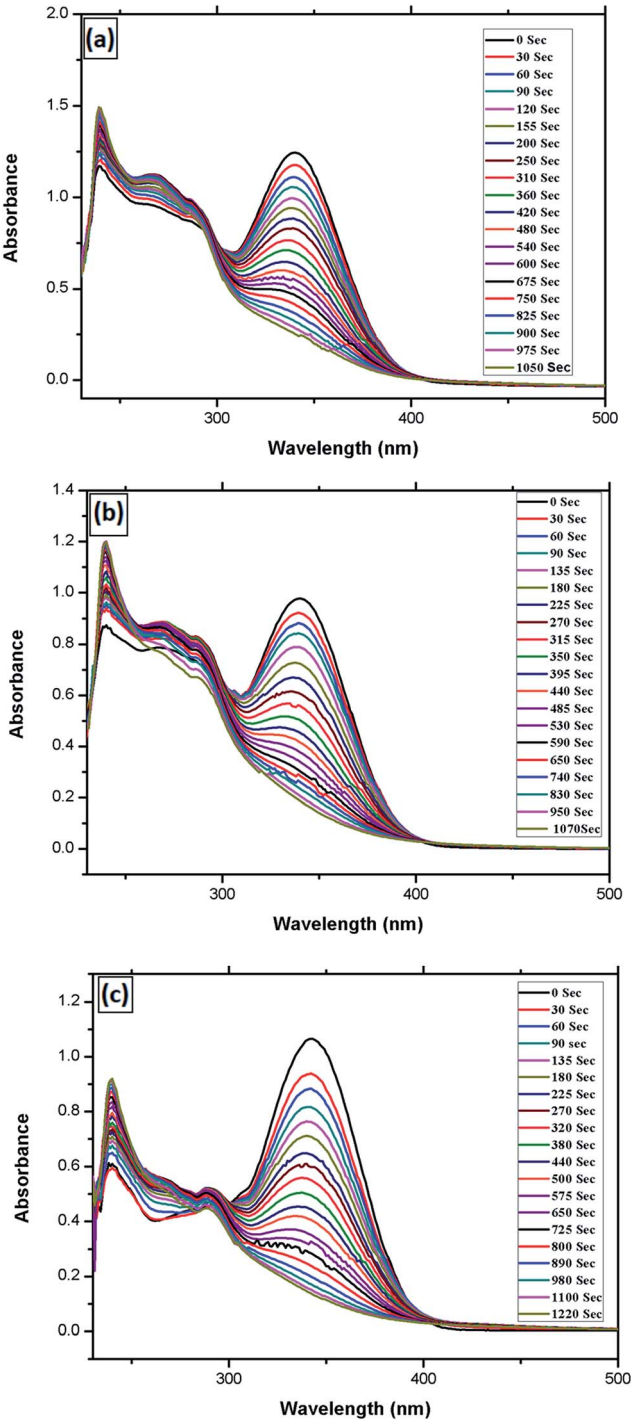

Fig. 5 Absorption spectra of the chalcones showing changes in absorption characteristics during UV-irradiation (CH-5 (a), CH-6 (b) and CH-10 (c)).

which also indicates that the chalcones have undergone photo-cross-linking. The absorbance spectra in Fig. 5 also show that CH-10 takes more time for photo-cross-linking than CH-5 and CH-6. This implies that the substituents of chalcone derivatives have significantly effect on the rate of photo-cross-linking. The rate of photo-cross-linking decreases with increase in the length of the aliphatic spacer that links the chalcone and triazole units.

As the spacer length increases, the distance between the chalcone and triazole units increases which might decrease the rate of photo-cross-linking.[17]

3.3. Potentiodynamic polarization measurements

The kinetics of anodic and cathodic reactions on MS surfaces in 1.0 M HCl solution without and with different concentrations of intact chalcones (CH-5, CH-6 and CH-10) and photo-cross-linked chalcones (CH-5c, CH-6c and CH-10c) were studied using potentiodynamic polarization measurements. The resulting polarization curves are shown in Fig. 6. It can be seen from Fig. 6 that the polarization curves shifted to either more cathodic or anodic region in the presence of the inhibitors compared to the blank acid system. This implies that the inhibitors adsorbed on mild steel surface thereby changing the electrochemical nature of the surface. More so, the polarization curves shifted to lower current density regions in the presence of the inhibitors (both intact and photo-cross-linked chalcones). One apparent feature of the polarization curves in Fig. 6 is that the polarization curves in the presence of the intact chalcones are similar to that of the blank acid system, which implies that the intact chalcones inhibit mild steel corrosion only by blocking some active sites on the steel surface without changing the actual mechanism of the corrosion reaction.[27] However, in the presence of the photo-cross-linked chalcones, the anodic arms of the polarization curves exhibit different features attributable to change in mechanism, which is more pronounced for CH-10 than CH-5 and CH-6. This implies that apart from reducing the corrosion rate, the photo-cross-linked inhibitors also alter the mechanism of anodic dissolution. Though, the actual mechanism cannot be ascertained. It can also be assumed that the extent of change in the anodic dissolution mechanism is proportional to the photo-cross-linking ability of the studied chalcones.

Electrochemical kinetic parameters such as E_{corr}, I_{corr}, b_a and b_c obtained by the extrapolation of the straight Tafel regions of the polarization curves to the E_{corr} are presented in Table 1. It is observed from Table 1 that the shift in E_{corr} for all the inhibitors is far less than 85 mV, which suggests that the studied chalcone derivatives (both intact and photo-cross-linked) are mixed-type inhibitors.[27] That is, the inhibitors reduce both the rates of anodic mild steel dissolution and cathodic hydrogen evolution reactions of mild steel in 1 M HCl. The values of the anodic and cathodic Tafel slopes do not reveal a predominant anodic or cathodic inhibition, which also supports the fact that the inhibitors are mixed-type in their activities. The inhibition efficiencies increase with increasing concentration for both the intact and photo-cross-linked chalcones. The inhibition efficiency (IE) of 99% was achieved with 15 ppm of the photo-cross-linked chalcone (CH-10c), but 15 ppm of the intact chalcone (CH-10) gives 96% of inhibition efficiency. The photo-cross-linked chalcone derivatives generally give higher IE than the intact chalcone derivatives because they have undergone structural modification which has increased their molecular size/volume compared to their corresponding intact chalcone derivatives. This implies that the photo-cross-linked chalcone

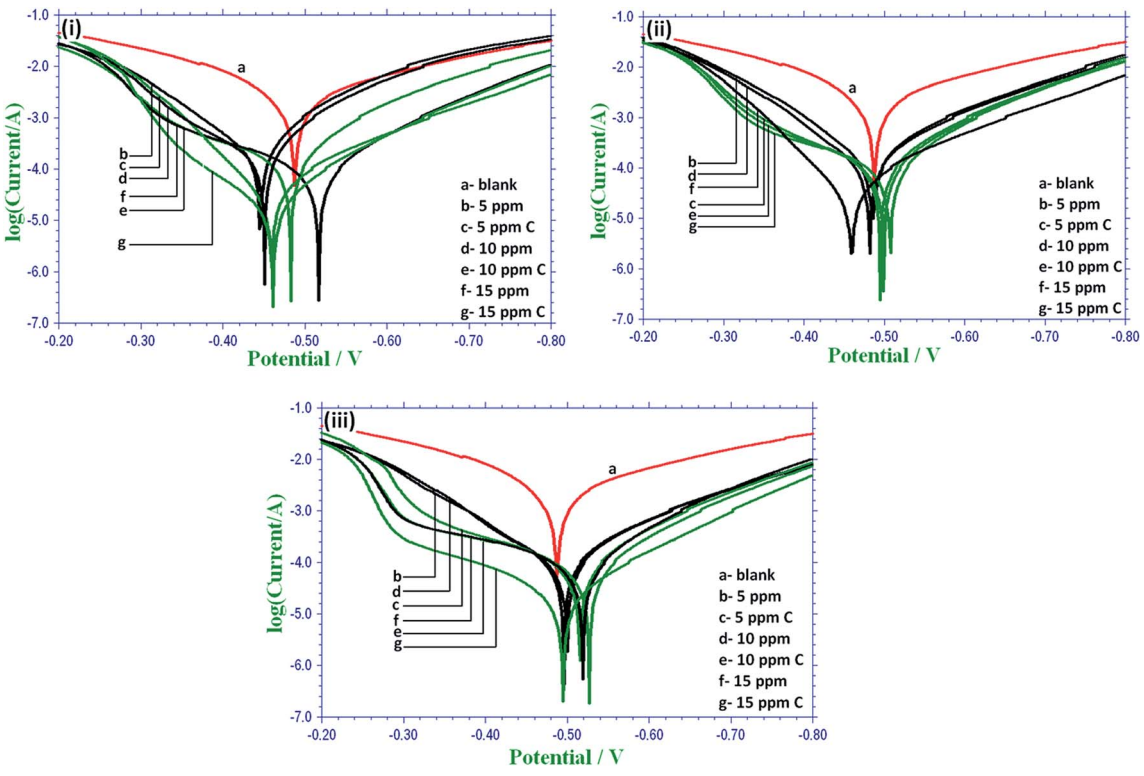

Fig. 6 Potentiodynamic polarization curves of MS in 1.0 M HCl without and with various concentrations of the inhibitors (CH-5 (i), CH-6 (ii) and CH-10 (iii)).

Table 1 Tafel polarization parameter values for the corrosion of MS in 1.0 M HCl in presence and absence of inhibitors

Inhibitor	Concentration of inhibitor (ppm)	I_{corr} ($\mu A\ cm^{-2}$)	$-E_{corr}$ (mV *vs.* SCE)	b_c (mV per decade)	b_a (mV per decade)	θ	IE (%)
Blank	0	2945	0.487	4.67	6.03	—	—
CH-5	5	269	0.445	8.51	11.04	0.909	90.9
	10	173	0.483	9.267	5.35	0.941	94.1
	15	113	0.517	8.35	4.89	0.962	96.2
CH-5c	5	225	0.451	8.53	9.76	0.923	92.3
	10	35	0.459	7.12	15.99	0.988	98.8
	15	21	0.461	9.04	11.71	0.993	99.3
CH-6	5	174	0.486	7.93	11.06	0.941	94.1
	10	127	0.482	8.10	12.13	0.957	95.7
	15	122	0.499	8.80	5.76	0.958	95.8
CH-6c	5	132	0.495	8.66	6.62	0.957	95.5
	10	127	0.508	9.12	4.46	0.955	95.8
	15	35	0.495	7.12	15.99	0.988	98.8
CH-10	5	108	0.496	7.07	10.67	0.963	96.3
	10	106	0.500	7.17	10.39	0.964	96.4
	15	107	0.519	8.72	4.20	0.964	96.4
CH-10c	5	111	0.516	8.08	4.55	0.962	96.2
	10	93	0.527	8.31	4.40	0.968	96.8
	15	27	0.495	8.72	5.56	0.991	99.1

molecules will exhibit a wider coverage area over the metal surface than the corresponding intact chalcone molecules.[17–19]

3.4. Electrochemical impedance spectroscopy (EIS)

The Nyquist plots for MS in 1.0 M HCl solution in the presence and absence of various concentrations of the inhibitors are shown in Fig. 7. The Nyquist plots show single semicircles which implies that the dissolution of mild steel in 1 M HCl without or with various concentrations of the studied inhibitors is controlled by single charged transfer process.[38] The depression of the Nyquist semicircles is often associated with the frequency dispersion of interfacial impedance arising from inhomogeneity

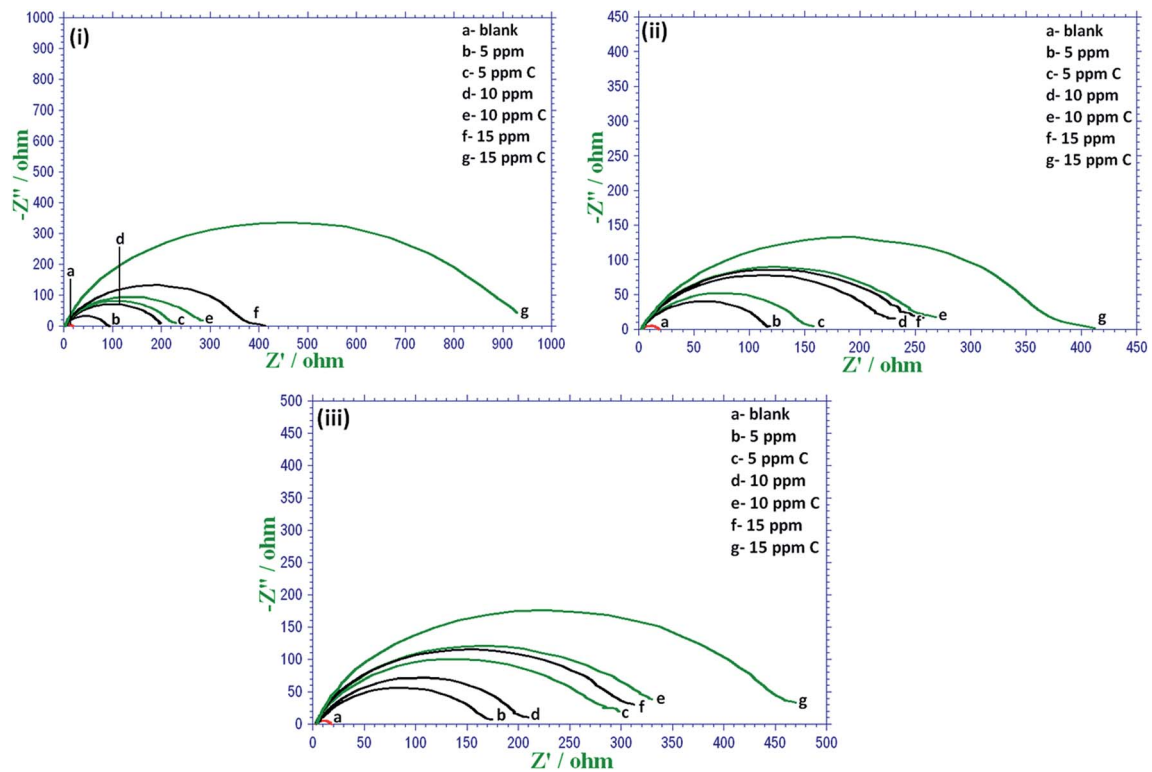

Fig. 7 Nyquist plots of MS in 1.0 M HCl without and with various concentrations of the inhibitors (CH-5 (i), CH-6 (ii) and CH-10 (iii)).

Table 2 Electrochemical impedance parameter values for the corrosion of MS in 1.0 M HCl in presence and absence of inhibitors

Inhibitor	Concentration of inhibitor (ppm)	R_{ct} (Ω cm^2)	f_{max}	C_{dl} (μF cm^2)	θ	IE (%)
Blank	0	16.8	32.8	498.80	—	—
CH-5	5	89.4	54.5	6.53	0.812	81.2
	10	199.5	58.2	2.74	0.916	91.6
	15	415.9	62.4	1.23	0.959	95.9
CH-5c	5	222.6	61.2	2.34	0.925	92.5
	10	280.8	62.5	1.81	0.940	94.0
	15	932.9	69.5	4.91	0.981	98.1
CH-6	5	115.8	53.6	5.13	0.855	85.5
	10	230.9	55.9	2.47	0.927	92.7
	15	250.8	60.4	2.10	0.933	93.3
CH-6c	5	160.7	59.7	3.32	0.895	89.5
	10	270.6	60.5	1.95	0.938	93.8
	15	410.3	62.5	1.24	0.959	95.9
CH-10	5	170.6	52.4	3.56	0.902	90.2
	10	210.1	55.4	2.74	0.920	92.0
	15	311.9	63.6	1.61	0.946	94.6
CH-10c	5	300.5	62.5	1.69	0.944	94.4
	10	332.7	64.6	2.77	0.949	94.9
	15	470.9	67.2	1.01	0.964	96.4

of the electrode surface due to roughness and/or other interfacial phenomena.[39,40]

The impedance spectra were fitted to the $R_s(R_{ct}CPE)$ equivalent circuit and the impedance parameters obtained from the fitting are presented in Table 2. The values of the double layer capacitance (C_{dl}) were calculated from the R_{ct} values using the equation:

$$C_{dl} = \frac{1}{(2\pi f_{max} R_{ct})} \quad (5)$$

where f_{max} is the frequency value at which the imaginary component of the impedance is maximum ($-Z_{max}$). The results in Table 2 show that the R_{ct} values increase with increasing concentration of the inhibitors and the C_{dl} values for the inhibitor-containing systems are generally lower than that of the acid blank, which suggest that the inhibitor adsorb on the steel surface thereby forming a protective layer on the steel surface and reducing the rate of charge transfer process. Similarly, the corrosion inhibition efficiency increases with increase in concentration of the inhibitors with the photo-cross-linked chalcones having higher inhibition efficiencies than the intact chalcones. The results show that the inhibition efficiencies obtained from the impedance study are in good agreement with those from polarization measurements.

3.5. Adsorption isotherm

Adsorption of a corrosion inhibitor on metal surface can occur through physisorption or chemisorption mechanism or a competitive form of both mechanisms. In general, physisorption is considered to be an exothermic process while chemisorption is an endothermic process. After adsorption, an inhibitor retards the rate of the cathodic and/or anodic electrochemical corrosion reaction. The mode of interaction between an organic compound and a metal surface can be deduced from adsorption isotherms. The experimental data

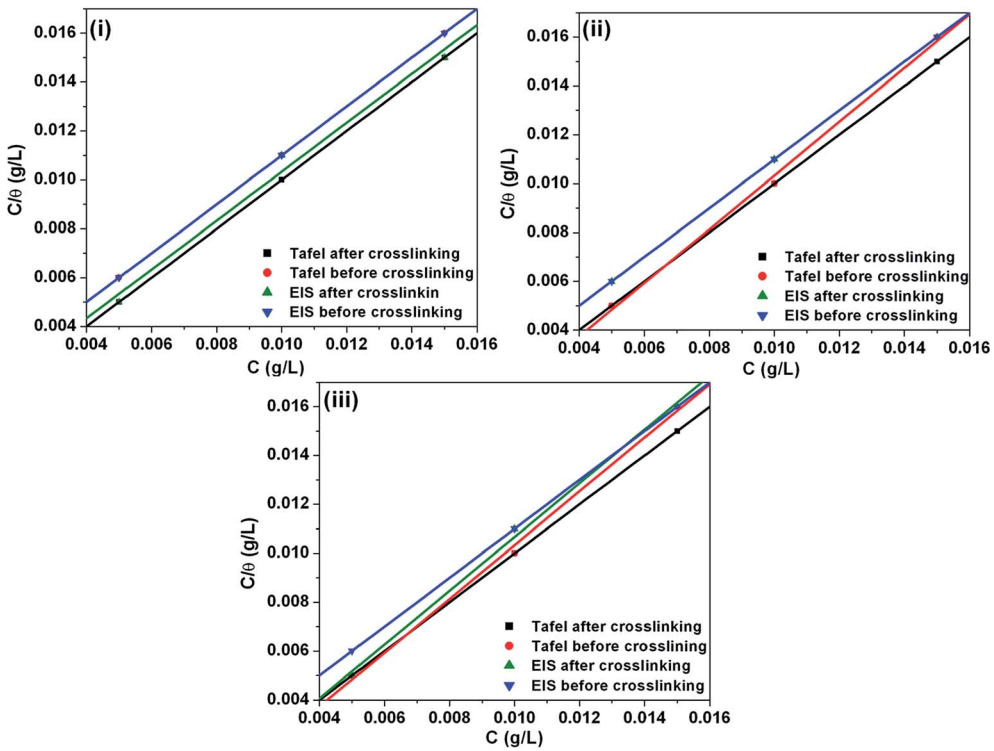

Fig. 8 Langmuir adsorption isotherm plots for CH-5 (i), CH-6 (ii) and CH-10 (iii).

obtained from both potentiodynamic polarization and EIS measurements were tested with different adsorption isotherms including Temkin, Langmuir, Frumkin and Freundlich isotherms. Langmuir adsorption isotherm was adjudged to give the best fit based on the correlation coefficient (R^2) values. The linear form of the Langmuir adsorption isotherm given by the equation:

$$\frac{C}{\theta} = \frac{1}{K_{ads}} + C \quad (6)$$

was used where K_{ads} is the equilibrium constant of the adsorption process and C is the inhibitor concentration. The plots C/θ against C for the intact and photo-cross-linked chalcones are shown in Fig. 8. The slight deviations of the slopes of the Langmuir plots from unity are due to the interactions between the adsorbed molecules on the metal surface as well as change in the heat of adsorption with increasing surface coverage.[41] The adsorption equilibrium constant, K_{ads} is related to the change in Gibbs free energy of adsorption (ΔG_{ads}) as:

$$\Delta G_{ads} = -RT \ln(55.5 K_{ads}) \quad (7)$$

where R is the gas constant (8.314 J K^{-1} mol^{-1}), T is the absolute temperature and 55.5 is the concentration of water solution. Thermodynamic parameters for the adsorption process obtained from Langmuir adsorption isotherm are given in Table 3. The negative values of ΔG_{ads} imply that the adsorption of the chalcones on mild steel surface is a spontaneous process. Generally, the values of ΔG_{ads} up to -20 kJ mol^{-1} are attributed to physisorption while those around -40 kJ mol^{-1} or more negative are associated with chemisorption process.[42,43] The ΔG_{ads} values obtained in this study are between -39.8 kJ mol^{-1} and -26.6 kJ mol^{-1} which imply that adsorption may involve competitive physisorption and chemisorption.

3.6. SEM-EDX studies

The formation of protective layer of inhibitors on MS surface was confirmed by SEM micrographs. The SEM images of the freshly polished MS specimen and MS specimens in 1.0 M HCl without and with the studied inhibitors are shown in Fig. 9. The surface morphology of freshly polished MS specimen (Fig. 9a) show smooth and pit-free surface. The image in Fig. 9b shows that the MS specimen in 1.0 M HCl solution without the inhibitors is highly damaged and characterized with a lot of pits due to direct acid attack. However, the effect of the inhibitors can be seen from Fig. 9c (CH-5) and Fig. 9d (CH-5c) in which the MS surfaces are not as damaged as in the case of the blank acid system. This implies that the studied inhibitors formed protective film on the steel surface thereby protecting it from direct acid attack.

Table 3 Adsorption parameters determined for chalcones investigated as inhibitor of mild steel corrosion in 1.0 M HCl

		Langmuir isotherm			
Method	Inhibitor	R^2	Slope	ΔG_{ads} (kJ g^{-1})	K_{ads} (kJ g^{-1}) $\times 10^3$
EIS	CH-5	1.000	0.948	−26.6	0.7
Tafel		1.000	1.009	−29.3	2.9
EIS	CH-5c	0.999	0.989	−28.9	1.8
Tafel		1.000	0.969	−29.0	1.9
EIS	CH-6	0.999	1.023	−28.4	1.5
Tafel		0.999	0.996	−32.6	7.7
EIS	CH-6c	1.000	1.006	−28.8	1.7
Tafel		1.000	1.037	−39.8	3.0
EIS	CH-10	1.000	1.031	−29.5	2.3
Tafel		1.000	1.037	−39.8	1.4
EIS	CH-10c	0.999	1.026	−31.5	5.0
Tafel		0.999	0.994	−30.6	3.5

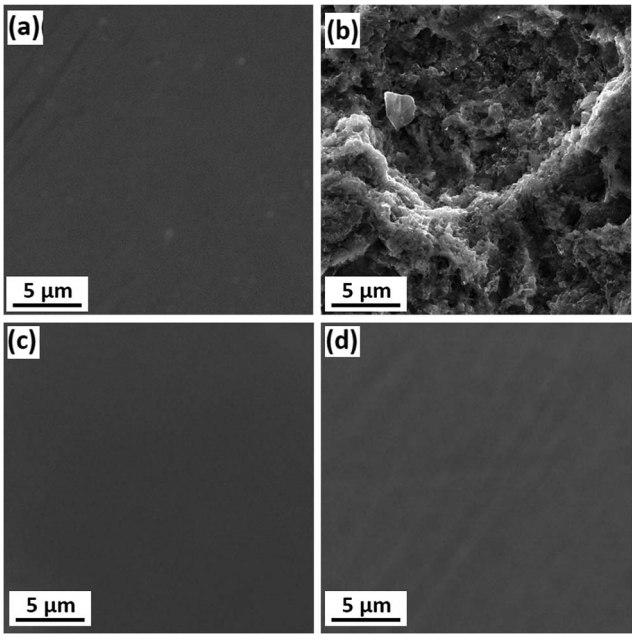

Fig. 9 SEM images of MS surface: (a) polished (b) in 1.0 M HCl without inhibitor (c) in 1.0 M HCl with 15 ppm intact inhibitor (CH-5), and (d) in 1.0 M HCl with 15 ppm photo-cross-linked inhibitor (CH-5c).

The EDX spectra were used to determine the elements present on MS surface before and after the exposure to the aggressive solutions without and with the studied inhibitors. The results of the EDX spectra shown in Fig. 10 are for the freshly polished MS surface and MS surface exposed to 1.0 M HCl solution in absence and presence of the inhibitors. The EDX spectra give atomic composition of the MS and the results are tabulated in Table 4. Freshly polished MS specimen (Fig. 10a) was smooth without chlorine content. However, the EDX spectrum of the MS specimen in 1 M HCl blank solution showed intense chlorine peaks due to the adsorbed chloride ions on the steel surface.[44] In the presence of inhibitors, the EDX spectra showed peaks for nitrogen atoms. This is due to the presence of nitrogen atom in the inhibitor molecule which is adsorbed on the MS surface. Also, the carbon peak is significantly increased due to the carbon atoms present in the adsorbed inhibitor species. The photo-cross-linked chalcone derivative (CH-5c) showed lower chloride ion adsorption indicating that the photo-cross-linked chalcone derivatives exhibit better corrosion inhibition potentials than the intact chalcones.

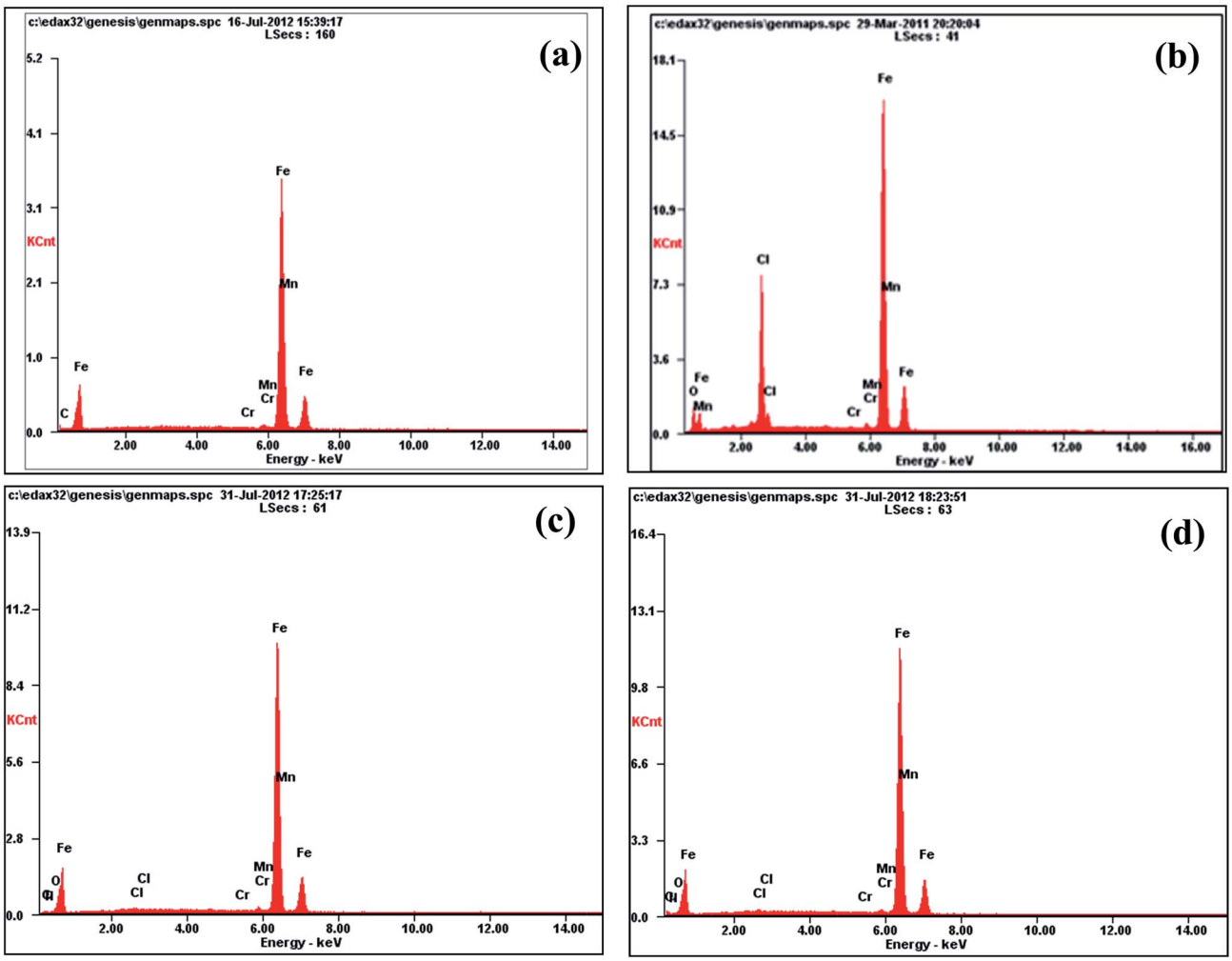

Fig. 10 EDX spectra of MS surface: (a) polished (b) in 1.0 M HCl without inhibitor (c) in 1.0 M HCl with 15 ppm intact inhibitor (CH-5), and (d) in 1.0 M HCl with 15 ppm photo-cross-linked inhibitor (CH-5c).

Table 4 Percentage atomic contents of elements on mild steel surface obtained from EDX analysis

	Composition						
Medium	Fe	O	C	Cl	Mn	Cr	N
Mild steel (a)	99.34	—	0.10	—	0.34	0.22	—
Mild steel in 1.0 M HCl (b)	76.32	9.83	—	13.12	0.32	0.41	—
CH3-5	90.95	2.37	3.86	0.64	1.05	0.12	1.01
CH3-5c	90.50	2.27	4.91	0.57	1.0	0.13	0.61
CH3-6	93.58	1.90	2.36	0.61	1.05	0.10	0.40
CH3-6c	93.00	2.05	2.83	0.51	1.02	0.15	0.45
CH3-10	91.90	2.07	3.37	0.58	1.23	0.19	0.66
CH3-10c	94.15	1.84	1.95	0.37	1.09	0.13	0.47

3.7. Quantum chemical results

The optimized geometries of the studied chalcone derivatives are shown in Fig. 10. All the quantum chemical data that are used for comparison with experimental results relate only to the lowest-energy conformer of each of the chalcone derivatives. The chemical reactivity of the chalcones was investigated by analyzing the frontier molecular orbitals. According to the frontier molecular orbital theory, chemical reactivity is strongly determined by the interaction of the highest occupied molecular orbital (HOMO) and the lowest unoccupied molecular orbital (LUMO) of the interacting species.[45] The HOMO graphical surfaces of the studied compounds are shown in Fig. 11. In all the structures, the HOMO (Fig. 11) is strongly delocalized on ring A and the double bond corresponding to the sites with the highest electron density.

Other quantum chemical parameters were computed to have more insight in the reactivity and selectivity of the chalcone dimers. The frontier molecular orbital energies (*i.e.*, E_{HOMO} and E_{LUMO}) provide information on the reactivity of chemical species. The E_{HOMO} is often associated with the electron donating ability of a molecule[46–48] and a higher E_{HOMO} energy value indicates higher tendency of the molecule to donate electron(s) to the appropriate acceptor molecule with low energy and empty/partially filled molecular orbital. The results in

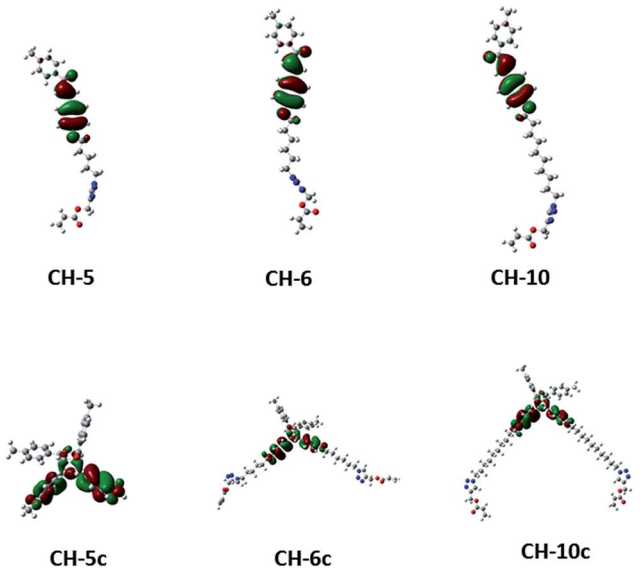

Fig. 11 HOMO graphical surfaces of the isolated and dimerised (photo-cross-linked) chalcones.

Table 5 show that the values of the E_{HOMO} for the photo-cross-linked chalcones are higher than those of the intact chalcones indicating that the photo-cross-linked chalcones have greater electron donating ability than the isolated chalcones. Therefore on interaction with the metal surface, the photo-cross-linked chalcones have greater tendency to donate electrons to the surface of the metal and therefore would have the better adsorption and greater inhibition potential. This result is in agreement with the experiment findings.

Absolute hardness (η) and softness (σ) are properties that also facilitate the analysis of the molecular reactivity and selectivity. The relationship between these quantum chemical quantities and corrosion inhibition is often based on the Lewis theory of acid and bases and Pearson's hard and soft acids and bases.[49] The band gap, ΔE (*i.e.*, the energy difference between the E_{LUMO} and E_{HOMO}) also provides information about the reactivity of the studied molecules. A hard molecule has a large ΔE while a soft molecule has a small ΔE. Soft molecules therefore could easily offer electrons to an acceptor system what makes them more reactive than hard molecules. In this regard, adsorption could occur at the region of the molecule where, σ has the highest value.[50] The values of σ reported in Table 5 show that the isolated chalcone derivatives have higher values of σ than the respective photo-cross-linked dimeric chalcone derivatives, which suggests that the values of σ do not correlate with the trend of the experimental inhibition efficiency.

The dipole moment (μ) is another index that is often used for the prediction of the direction of a corrosion inhibition process. It is the measure of polarity in a bond and is related to the distribution of electrons in a molecule.[51] Inhibitors with high dipole moment tend to form strong dipole–dipole interactions with the metal, resulting in strong adsorption on the surface of the metal and therefore leading to greater inhibition efficiency.[52] However, a survey of literature shows that in most cases, experimental inhibition efficiencies do not always correlate with dipole moments.[52] The results reported in Table 5 suggest that the trend in the dipole moment does not follow the trend of the observed inhibition efficiency.

Therefore, of all the quantum chemical parameters, only the energy of the E_{HOMO} may account for explaining the difference in the inhibition efficiency between the isolated chalcone derivatives and the photo-cross-linked chalcone derivatives. This is not a surprising phenomenon considering that an attempt to correlate individual quantum chemical parameters to the experimental inhibition efficiencies of the inhibitors do not always reveal an optimal correlation.[53] In such cases, it is often useful to resort to the quantitative structure property relationship (QSPR) in which several quantum chemical parameters form a composite index that is then correlated to the experimentally determined inhibition efficiency.[54] However, that approach has not been tested here because of the few number of inhibitor molecules considered in this study. The results of the quantum chemical calculations reported here have therefore provided information about the possible sites on the studied molecules that could be involved in an electrophilic attack as well as identified the fact that apart from E_{HOMO}, all other estimated quantum chemical parameters cannot be utilized individually to explain the trend of the experimental inhibition efficiency.

3.8. Monte Carlo simulations

Fig. 12 shows a typical plot of energy distribution for CH-10 with Fe (110) surface during energy optimization process. Also Fig. 13 depicts a typical adsorption energy profile as CH-10

Table 5 The calculated molecular properties for the studied isolated chalcones and the dimeric (photo-cross-linked) chalcones B3LYP/6-31+G (d, p) results *in vacuo*

Quantum chemical parameters	Intact chalcones			Dimeric (photo-cross-linked) chalcones		
	CH-5	CH-6	CH-10	CH-5c	CH-6c	CH-10c
E_{HOMO} (eV)	−5.846	−5.814	−5.762	−5.517	−5.605	−5.554
E_{LUMO} (eV)	−1.902	−1.88	−1.846	−1.545	−1.618	−1.543
ΔE (eV)	3.944	3.935	3.916	3.973	3.986	4.011
μ (debye)	3.554	5.830	4.938	4.302	6.699	4.122
Hardness (η)	1.972	1.967	1.958	1.986	1.993	2.005
Softness (σ)	0.507	0.508	0.511	0.504	0.502	0.499

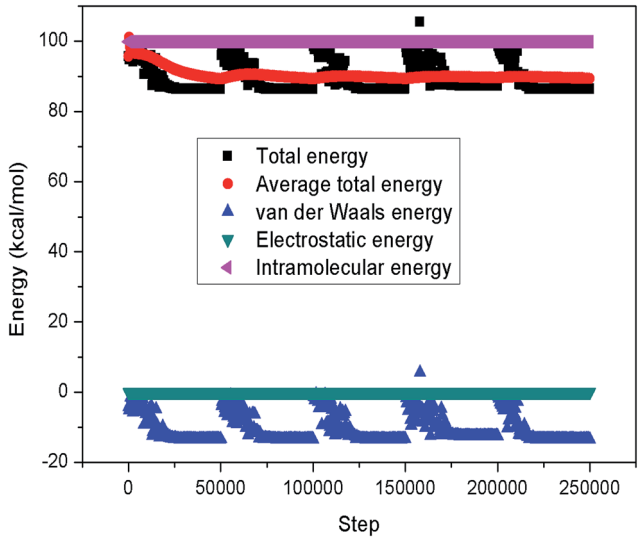

Fig. 12 Typical energy profile plots for CH-10/Fe (110)/system obtained during 5 cycles of the Monte Carlo simulation process.

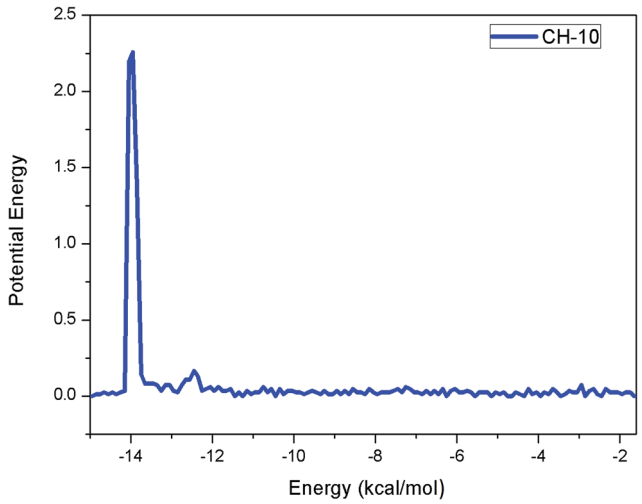

Fig. 13 Typical adsorption energy profile for CH-10 interaction with Fe (110) surface.

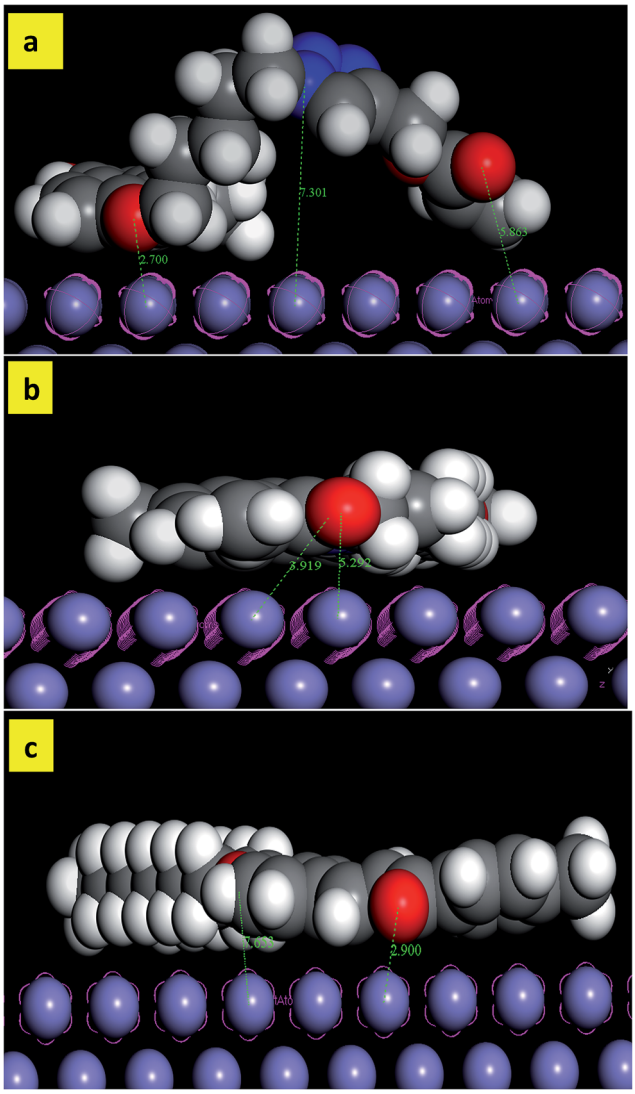

Fig. 14 Snapshots of the most stable low energy configuration for the adsorption of (a) CH-5, (b) CH-6 and (c) CH-10 on Fe (110) surface.

interacts with Fe. The most stable low energy adsorption configurations of the inhibitors on Fe (110) surface using Monte Carlo simulations are depicted in Fig. 14(a–c). The bond distances between the closest heteroatoms of the inhibitors and Fe (110) surface at equilibrium were as follows: CH-5–Fe interaction: (Fe–O = 2.700 Å); CH-6–Fe interaction: (Fe–O = 3.919 Å); CH-10–Fe interaction: (Fe–O = 2.900 Å). These bond distances, which are greater than the average Fe–O bond length suggest that the adsorption of the studied inhibitors on iron surface is predominantly through electrostatic interactions between the inhibitors and Fe, *i.e.* physical adsorption. Though, this does not totally preclude the possibility of chemisorption as the experimental data revealed the possibility of competitive physisorption and chemisorption mechanisms. It is clear also from Fig. 14 that CH-10 adsorbed in a totally flat manner on Fe surface, which enhances its surface coverage on the metal when compared to CH-5 and CH-6.

The values for the adsorption energies obtained as output from MC simulation are listed in Table 6. It is quite clear from Table 6, that the adsorption energies of the inhibitors on iron surface decreased in the following order CH-10 > CH-6 > CH-5. It is generally acknowledged that the primary mechanism of corrosion inhibitor interaction with steel is by adsorption. So the adsorption energy can provide us with a direct tool to rank

Table 6 Adsorption energies of CH-5, CH-6 and CH-10 on Fe (110) surface (all results in kcal mol^{-1})

Systems	Adsorption energy
Fe (110)/CH-5	−9.44
Fe (110)/CH-6	−12.14
Fe (111)/CH-10	−14 to 84

inhibitor molecules. High negative adsorption energy indicates the system with the most stable and stronger adsorption.[55–57] This ordering is the same as the experimental determined inhibition efficiencies for the investigated chalcones. The result also shows the effect of increasing chain length on the performance of the chalcones investigated.

4. Conclusions

In conclusion, new chalcone derivatives with photo-cross-linking characteristics were successfully synthesized by click-chemistry and characterized using FTIR and NMR spectroscopic techniques. The synthesized chalcones undergo photo-cross-linking upon irradiation with mercury lamp and this was confirmed by the UV-vis absorption spectra. Potentiodynamic polarization measurements showed that the chalcone derivatives are mixed type corrosion inhibitors. EIS measurements revealed that the chalcone derivatives form protective film on mild steel surface thereby reducing the rate of charge transfer process. The inhibition efficiencies increase with increase in concentration of the chalcones. The photo-cross-linked chalcones show higher inhibition potentials that their corresponding intact chalcones. Adsorption of the chalcones on MS surface obeyed the Langmuir adsorption isotherm and the values of ΔG revealed the possibility of competitive physisorption and chemisorption processes. Among the quantum chemical properties, the energy of the HOMO provides a better explanation for the higher inhibition efficiency of the photo-cross-linked chalcone derivatives compared to the intact chalcones. The Fe–O bond distances obtained from Monte Carlo simulation studies also suggested that the adsorption of the studied chalcones on Fe surface is mainly physisorption. The results obtained from the theoretical studies provide good corroborative explanations of the experimental results.

Acknowledgements

R. Baskar, S. Yesudass, A. S. Adekunle and I. Bahadur are grateful to the North-West University, South Africa for granting them Postdoctoral Fellowships enabling them to participate in this work. L. O. Olasunkanmi gratefully acknowledges NRF/Sasol Inzalo foundation for support towards his PhD studies. I. B. Obot thanks the Center of Research Excellence in Corrosion, King Fahd University of Petroleum and Minerals (KFUPM) for support in carrying out the Monte Carlo simulations using Material studio 7.0 software licensed by Accelrys Inc. USA. E. E. Ebenso thanks the National Research Foundation (NRF) of South Africa for funding.

References

1 D. M. Strickland, *Ind. Eng. Chem.*, 1923, **15**, 566–569.
2 J. D. Hatfield, A. V. Slack, G. L. Crow and H. B. Shaffer, *J. Agric. Food Chem.*, 1958, **6**, 524–531.
3 B. G. Clubley, *Chemical Inhibitors for Corrosion Control*, Royal Society of Chemistry, Cambridge, 1990.
4 G. Subhadra, G. Saraswathi, P. Jaisankar, J. K. Singh and A. Elango, *Corros. Sci.*, 2012, **60**, 193–204.
5 G. Ji, S. K. Shukla, P. Dwivedi, S. Sundaram and R. Prakash, *Ind. Eng. Chem. Res.*, 2011, **27**, 11954–11959.
6 M. Bouayed, H. Rabaa, A. Srhiri, J. Y. Saillard, A. B. Bachiran and A. L. Beuze, *Corros. Sci.*, 1999, **41**, 501–517.
7 P. Bommersbach, C. A. Dumont, J. P. Millet and B. Normand, *Electrochim. Acta*, 2005, **51**, 1076–1084.
8 A. Popova, S. Raicheva, E. Sokolova and M. Christov, *Langmuir*, 1996, **12**, 2083–2089.
9 L. C. Murulana, M. M. Kabanda and E. E. Ebenso, *RSC Adv.*, 2015, **5**, 28743–28761.
10 M. Bouayed, H. Rabaa, A. Srhiri, J. Y. Saillard, A. B. Bachiran and A. L. Beuze, *Corros. Sci.*, 1999, **41**, 501–517.
11 P. Bommersbach, C. A. Dumont, J. P. Millet and B. Normand, *Electrochim. Acta*, 2005, **51**, 1076–1084.
12 D. T. Ortega, T. Pandiyan, J. Cruz and E. G. Ochoa, *J. Phys. Chem. C*, 2007, **27**, 9853–9866.
13 R. Gaur, V. K. Gupta, A. Pal, M. P. Darokar, R. S. Bhakuni and B. Kumar, *RSC Adv.*, 2015, **5**, 5830–5845.
14 K. Revathy and A. Lalitha, *RSC Adv.*, 2014, **4**, 279–285.
15 X. D. Li, Z.-X. Zhong, J. J. Kim and M. H. Lee, *Macromol. Rapid Commun.*, 2004, **25**, 1090–1094.
16 Y. H. Qi, J. F. Ding, D. Michael, J. Jia and C. L. Callender, *Polymer*, 2006, **47**, 8263–8271.
17 R. Baskar, D. Kesavan, M. Gopiraman and K. Subramanian, *RSC Adv.*, 2013, **3**, 17039–17047.
18 R. Baskar, D. Kesavan, M. Gopiraman and K. Subramanian, *Prog. Org. Coat.*, 2014, **77**, 836–844.
19 R. Baskar, M. Gopiraman, D. Kesavan, K. Subramanian and S. Gopalakrishnan, *J. Mater. Eng. Perform.*, 2015, **24**, 2847–2856.
20 Y. R. Girish, K. S. S. Kumar, U. Muddegowda, N. K. Lokanath, K. S. Rangappa and S. Shashikanth, *RSC Adv.*, 2014, **4**, 55800–55806.
21 M. S. Gong, *Sens. Actuators, B*, 2010, **148**, 559–568.
22 D. H. Choi and S. J. Oh, *Eur. Polym. J.*, 2002, **38**, 1559–1564.
23 A. V. R. Reddy, K. Subramanian, V. Krishnaswamy and J. Ravichandran, *Eur. Polym. J.*, 1996, **32**, 919–926.
24 R. Baskar and K. Subramanian, *Spectrochim. Acta, Part A*, 2011, **79**, 1992–1997.
25 S. A. Abd El-Maksoud and A. S. Fouda, *Mater. Chem. Phys.*, 2005, **93**, 84–90.
26 J. Aljourani, K. Raeissi and M. A. Golozar, *Corros. Sci.*, 2009, **51**, 1836–1843.
27 R. Baskar, M. Gopiraman, D. Kesavan, I. S. Kim and K. Subramanian, *Ind. Eng. Chem. Res.*, 2012, **51**, 3966–3974.
28 A. D. Becke, *J. Chem. Phys.*, 1993, **98**, 5648–5652.
29 R. G. Parr and R. G. Pearson, *J. Am. Chem. Soc.*, 1983, **105**, 7512–7516.
30 M. J. Frisch, G. W. Trucks, H. B. Schlegel, G. E. Scuseria, M. A. Robb, J. R. Cheeseman, G. Scalmani, V. Barone, B. Mennucci, G. A. Petersson, H. Nakatsuji, M. Caricato, X. Li, H. P. Hratchian, A. F. Izmaylov, J. Bloino, G. Zheng, J. L. Sonnenberg, M. Hada, M. Ehara, K. Toyota, R. Fukuda, J. Hasegawa, M. Ishida, T. Nakajima, Y. Honda, O. Kitao, H. Nakai, T. Vreven, J. A. Montgomery Jr,

J. E. Peralta, F. Ogliaro, M. Bearpark, J. J. Heyd, E. Brothers, K. N. Kudin, V. N. Staroverov, R. Kobayashi, J. Normand, K. Raghavachari, A. Rendell, J. C. Burant, S. S. Iyengar, J. Tomasi, M. Cossi, N. Rega, J. M. Millam, M. Klene, J. E. Knox, J. B. Cross, V. Bakken, C. Adamo, J. Jaramillo, R. Gomperts, R. E. Stratmann, O. Yazyev, A. J. Austin, R. Cammi, C. Pomelli, J. W. Ochterski, R. L. Martin, K. Morokuma, V. G. Zakrzewski, G. A. Voth, P. Salvador, J. J. Dannenberg, S. Dapprich, A. D. Daniels, O. Farkas, J. B. Foresman, J. V. Ortiz, J. Cioslowski, and D. J. Fox, *Gaussian 09, Revision C.01*, Gaussian, Inc., Wallingford CT, 2009.

31 K. F. Khaled, *J. Solid State Electrochem.*, 2009, **13**, 1743–1756.

32 J. J. Fu, H. S. Zang, Y. Wang, S. N. Li, T. Chen and X. D. Liu, *Ind. Eng. Chem. Res.*, 2012, **51**, 6377–6386.

33 A. B. Anderson and S. P. Mehandru, *Surf. Sci.*, 1984, **136**, 398–418.

34 L. O. Olasunkanmi, I. B. Obot, M. M. Kabanda and E. E. Ebenso, *J. Phys. Chem. C*, 2015, **119**, 16004–16019.

35 A. K. Satapathy, G. Gunasekaran, S. C. Sahoo, A. Kumar and P. V. Rodrigues, *Corros. Sci.*, 2009, **51**, 2848–2856.

36 H. R. Allcock and C. G. Cameron, Grant: N00014-91-J- 1194.

37 R. Balaji and S. Nanjundan, *React. Funct. Polym.*, 2001, **49**, 77–86.

38 J. N. Asegbeloyin, P. M. Ejikeme, L. O. Olasunkanmi, A. S. Adekunle and E. E. Ebenso, *Materials*, 2015, **8**, 2918–2934.

39 M. E. Mashuga, L. O. Olasunkanmi, A. S. Adekunle, S. Yesudass, M. M. Kabanda and E. E. Ebenso, *Materials*, 2015, **8**, 3607–3632.

40 M. Hosseini, S. F. L. Mertens, M. Ghorbani and M. R. Arshadi, *Mater. Chem. Phys.*, 2003, **78**, 800–808.

41 A. Bouyanzer, B. Hammouti and L. Majidi, *Mater. Lett.*, 2006, **60**, 2840–2843.

42 R. F. V. Villamil, P. Corio, J. C. Rubim and S. M. L. Agostinho, *J. Electroanal. Chem.*, 1999, **472**, 112–119.

43 E. Khamis, F. Bellucci, R. M. Latanision and E. S. H. EI-Ashry, *Corrosion*, 1991, **47**, 677–686.

44 B. G. Ateya, B. E. EI-Anadouli and F. M. A. EI-Nizamy, *Corros. Sci.*, 1984, **24**, 497–568.

45 M. A. Amin, S. S. Abd El-Rehim, E. E. F. El-Sherbini and R. S. Bayoumi, *Electrochim. Acta*, 2007, **52**, 3588–3600.

46 M. M. Kabanda, S. K. Shukla, A. K. Singh, L. C. Murulana and E. E. Ebenso, *Int. J. Electrochem. Sci.*, 2012, **7**, 8813–8831.

47 M. M. Kabanda and E. E. Ebenso, *Int. J. Electrochem. Sci.*, 2012, **7**, 8713–8733.

48 R. G. Pearson, *Proc. Natl. Acad. Sci. U. S. A.*, 1986, **83**, 8440–8441.

49 M. M. Kabanda, L. C. Murulana, M. Ozcan, F. Karadag, I. Dehri, I. B. Obot and E. E. Ebenso, *Int. J. Electrochem. Sci.*, 2012, **7**, 5035–5056.

50 J. Malyszko and M. Scendo, *Monatsh. Chem.*, 1987, **118**, 435–443.

51 B. D. Mert, M. E. Mert, G. Kardaş and B. Yazici, *Corros. Sci.*, 2011, **53**, 4265–4272.

52 T. Arslan, F. Kandemirli, E. E. Ebenso, I. Love and H. Alemu, *Corros. Sci.*, 2009, **51**, 35–47.

53 E. E. Ebenso, M. M. Kabanda, L. C. Murulana, A. K. Singh and S. K. Shukla, *Ind. Eng. Chem. Res.*, 2012, **51**, 12940–12958.

54 L. C. Murulana, A. K. Singh, S. K. Shukla, M. M. Kabanda and E. E. Ebenso, *Ind. Eng. Chem. Res.*, 2012, **51**, 13282–13299.

55 W. Shi, M. Xia, W. Lei and F. Wang, *Desalination*, 2013, **322**, 137–143.

56 S. A. Umoren, I. B. Obot, A. M. Kumar and Z. M. Gasem, *J. Adhes. Sci. Technol.*, 2015, **29**(4), 271–295.

57 I. B. Obot, N. O. Obi-Egbedi, E. E. Ebenso, A. S. Afolabi and E. E Oguzie, *Res. Chem. Intermed.*, 2013, **39**, 1927–1948.

